Impact-parameter dependence of the relativistic photoeffect and other high-energy photoprocesses

Allan H. Sørensen
Institute of Physics and Astronomy, University of Aarhus, DK-8000 Aarhus C, Denmark
(Received 20 October 2000; published 31 May 2001)

The resolution in space of processes involving high-energy photons incident on atoms or bare atomic nuclei is investigated. A simple analysis, based on momentum transfer, gives first indications of the length scale being defined by the Compton wavelength of the electron for both the photoeffect and electron-positron pair creation with the electron bound to the atomic nucleus. Since the simple method of converting a momentum transfer q to a distance of $\hbar/q$ has potential pitfalls, we continue with a detailed wave-packet study. This study, which is undertaken for the case of the photoeffect, involves the incidence of a photon localized in space and time on a hydrogenlike atom. The wave-packet approach confirms the Compton wavelength, and not the extent of the atomic state, to be the decisive measure for photon energies in excess of the electron rest energy mc^2. In addition, it provides a direct and detailed picture of the impact-parameter dependence of the process. As an introduction to the wave-packet study, we compare calculations based on a plane-wave representation of the unbound lepton to lowest-order perturbative calculations.

DOI: 10.1103/PhysRevA.64.012703 PACS number(s): 32.80.Fb, 13.40.−f

I. INTRODUCTION

When discussing photoprocesses we often have a less clear picture of where in direct space they occur than is the case for processes involving only charged particles. As an example, consider the well-known photoelectric effect. In this process, an impinging photon is basically swallowed by the struck atom which, in return, emits an electron with an energy equal to the photon energy less the original binding energy of the electron. It seems natural to expect the conversion to take place in regions where there is a good chance to find the electron when in its original atomic state; that is, one could be tempted to predict that the spatial region involved in the conversion process corresponds to that covered by the electron cloud. However, this is generally not so. In the high-energy region, conversion takes place only in a much narrower region concentrated around the Coulomb center of the nucleus. The scale is the Compton wavelength of the electron.

In the following we shall shed some light on the question of the spatial extent of processes involving high-energy photons. We shall begin by the simplest possible analysis, that is, an analysis in terms of recoil momenta. This is the method usually applied in order to gain insight into the regions of space involved in various processes; see, e.g., Refs. [1–3]. In essence, the method boils down to a computation of the minimum momentum transfer q_{min} involved in the process under consideration and, subsequently, with recourse to, e.g., the Heisenberg uncertainty principle, conversion to a supposedly characteristic distance of $\hbar/q_{min}$. As it turns out, some of the results obtained in this way may seem counter intuitive. Furthermore, the method of converting momenta to distances is not infallible. For instance, for a negative τ lepton bound deeply inside a spherical nucleus, the bound-state energy is dictated with high precision by the behavior of the binding potential inside the nucleus, and yet the content of the wave function at large momenta by no means corresponds to the harmonic-oscillator form of the potential at short distances [4]. As another example we may mention that the so-called Bloch correction to the perturbative formula of Bethe, for the electronic stopping of a nonrelativistic charged particle penetrating matter, pertains to close collisions but at the same time appears at small scattering angles [5]. To avoid such pitfalls, we continue with a direct calculation of the impact-parameter dependence of the photoeffect. This calculation, which is the central part of the paper, proceeds by means of a wave-packet approach in which a photon localized in space and time impinges on a hydrogenlike atom in its ground state. As it turns out, the calculation confirms the result of the simple recoil analysis, insofar as it shows the length scale to be defined by the Compton wavelength at relativistic energies. But, in addition, it provides a very detailed insight into the impact-parameter dependence of the conversion process and its variations with, for instance, atomic number and primary energy. As a preamble to the wave-packet study, but also as a topic of broader interest, we shall discuss the quality of calculations based on a plane-wave representation of the emitted unbound lepton as compared to lowest-order perturbative calculations.

In addition to the photoeffect, we shall discuss the process by which an incoming photon converts in the field of a bare atomic nucleus to an electron-positron pair, with the electron produced directly in the ground state pertaining to the attractive interaction potential with the nucleus forming a hydrogenlike system. Below, this process will be termed ''bound-free pair creation.'' On a few occasions we shall also touch upon the creation of pairs of unbound particles, as well as on bremsstrahlung.

For reference we note that a theoretical investigation was recently reported concerning the emission, resolved in both space and time, of a photon by an atom; see Ref. [6]. As opposed to our treatment, this study was based on first-quantized theory, and aimed at photon energies much less than mc^2.

We use natural units ($\hbar = m = c = 1$, m being the electron mass) throughout. The Compton wavelength $\lambda\!\!\!^{-}_C = \hbar/mc$ is hence our unit of length.

 ©2001 The American Physical Society

II. ANALYSIS BASED ON RECOIL MOMENTA

In the photoelectric process a photon of energy k incident on an atom is absorbed, while an electron, originally bound in the atom with a binding energy $0<E_B<1$, is emitted with kinetic energy

$$E_k=k-E_B. \tag{1}$$

The magnitude of the momentum $\mathbf{p}$ of the outgoing electron is fixed by this energy as

$$p^2+1=(E_k+1)^2, \tag{2}$$

from which it is found that the final electron momentum exceeds the photon momentum $\mathbf{k}$ in magnitude for photon energies fulfilling the inequality

$$k>\frac{E_B(1-E_B/2)}{1-E_B}. \tag{3}$$

The right-hand side of Eq. (3), which varies monotonically with E_B, assumes values less than 0.3 for $E_B\leqslant 0.25$. This implies that at relativistic energies, we always find $p>k$.

The momentum transfer to the atom,

$$\mathbf{q}=\mathbf{k}-\mathbf{p}, \tag{4}$$

obviously assumes its minimum magnitude $q_{min}=|p-k|$ for parallel electron and photon momenta. The difference $p-k$ increases monotonically with the photon energy from $-E_B$ at threshold for the photoelectric effect to $1-E_B$ in the extreme high-energy limit, $k\to\infty$; the full increase is hence one momentum unit (mc). In the relativistic region we have, in particular,

$$\sqrt{(1-E_B)(3-E_B)}-1\leqslant q_{min}\leqslant 1-E_B, \quad k\geqslant 1. \tag{5}$$

The lower limit is larger than 0.43 for $E_B\leqslant 0.25$. Hence the minimum momentum transfer q_{min} always assumes values of order 1 for photon energies beyond 1.

The last finding has important implications. From arguments based on the Heisenberg uncertainty relations, or, similarly, from arguments on Fourier transforms, a momentum transfer in excess of mc is seen to imply characteristic distances of the order of the Compton wavelength of the electron, $\lambda\!\!\!^{-}_C$, our unit of length. This means that in the photoelectric effect, the conversion actually only takes place within distances of order $\lambda\!\!\!^{-}_C$ from the nucleus at relativistic energies—regardless of the fact that the electron may be found much further out. This was noted and utilized by Pratt *et al.* [3].

In bound-free pair creation, the minimum momentum transfer attains the value

$$q_{min}=k-p_+=k-\sqrt{(k-E_-)^2-1}. \tag{6}$$

Here index + refers to the outgoing positron, while the energy of the bound electron is $E_-=1-E_B$. The last step in Eq. (6) is obtained by energy conservation. The minimum momentum transfer [Eq. (6)] varies only moderately with the photon energy: it decreases monotonically by one unit (mc) from $1+E_-=2-E_B$ at threshold to, again, $E_-=1-E_B$ at infinity. With q_{min} of order 1, the process takes place within distances from the force center of the order of the Compton wavelength—exactly like the photoeffect.

For the case of creation of free pairs, the situation is different. The minimum momentum transfer obviously pertains to situations where the momenta $\mathbf{p}_+$ and $\mathbf{p}_-$ of the created positron and electron are colinear with that of the incident photon, i.e.,

$$q_{min}=k-p_+-p_-. \tag{7}$$

Applying energy conservation and introducing the parameter $\eta=E_+/k$, where E_+ denotes the energy of the positron, Eq. (7) may be rewritten as

$$q_{min}=k\{1-\eta\sqrt{1-1/(\eta k)^2}-(1-\eta)\sqrt{1-1/[(1-\eta)k]^2}\}. \tag{8}$$

Near threshold (which appears for $k=2$) the minimum momentum transfer is of order 1, but for high energies, $k\gg 1$, and η not too close to 0 or 1, Eq. (8) may be expanded to yield

$$q_{min}\simeq\frac{1}{2k\eta(1-\eta)}=\frac{k}{2E_+E_-}. \tag{9}$$

That is, for high energies (and η not too close to 0 or 1) the minimum momentum transfer attains values much smaller than 1. As it turns out, the cross-section differential in the momentum transfer becomes large at small values of q, and with $q_{min}\ll 1$ this means that momentum transfers much smaller than mc are important in the creation of free pairs. In turn, this implies that action at distances far beyond the Compton wavelength is of importance in the creation of free pairs by high-energy photons. In fact, distances as far as the atomic radius may come into play, and, as is well established, the decrease in q_{min} with increasing photon energy eventually leads to a limitation of cross sections due to atomic screening, that is, due to the finite range of the potential in which the conversion takes place.

Similar remarks apply to bremsstrahlung emission by electrons or positrons deflecting in atomic fields. Again, the minimum momentum transfer attains values much less than 1, and at sufficiently high energies saturation of the cross section due to atomic screening is encountered. Also see Ref. [7].

At this point, there is a fair chance to be left with somewhat uneasy feelings about the recoil method, not least due to the counterintuitive results obtained. In pair creation, for example, we have seen that while the creation of bound-free pairs only involves distances of order $\lambda\!\!\!^{-}_C$ from the nucleus, the creation of free pairs involves the entire atom in the high-energy limit. This could seem turned upside down, since it is in the bound-free pair creation that a specific atomic orbital is involved. Also, the conversion method may be questioned. For instance, arguments about behavior at small distances being reflected at large momenta are not always true. An example is provided by the ground state of a negatively charged τ lepton bound to a heavy nucleus in a

hydrogenlike system. The lepton moves well inside the nucleus. For a uniformly charged nucleus, which produces a harmonic-oscillator potential inside the nuclear radius, this is demonstrated very clearly by the fact that the exact ground-state energy deviates very little, for a uranium nucleus by only 0.01%, from the oscillator ground-state energy. Yet the behavior at large momenta is by no means that of the harmonic oscillator; the fall-off of the density in momentum space with increasing momentum is much slower than the rapid Gaussian decay pertaining to the oscillator; cf. Ref. [4].

Below we shall demonstrate the spatial structure for high-energy photo processes explicitly in a direct calculation of the impact-parameter dependence of the photoelectric effect. For the purpose of simplicity, we shall discuss hydrogenlike systems only, and we shall apply the simplest possible description of the outgoing electron, that is, a description in terms of plane waves.

III. LOWEST ORDER VS PLANE-WAVE APPROXIMATION

Before we turn to the actual calculation, a few words are in place as to the applicability of a plane-wave description. This discussion is of course not only interesting in the current context, but important in general for the study of high-energy photoprocesses.

At nonrelativistic energies, calculations to lowest order of the photoeffect proceed by means of a plane-wave description of the outgoing electron; cf. Ref. [7]. However, at relativistic energies such a description is insufficient for obtaining lowest-order results [3,8]. Here it is necessary to expand the wave function for the unbound electron to first order in αZ, α being the fine-structure constant. The cross section, correct to lowest order at relativistic energies, was first derived by Sauter [9]. Below we shall discuss the quality of the results obtained by the plane-wave description in comparison to those of Sauter. Recently, the plane-wave method was also applied in a computation of bound-free pair creation [4]. It is hence obviously of interest to extend the discussion of the quality of the plane-wave method to this case.

A. Bound-free pair production

Let us start by considering bound-free pair creation. By describing the electron in the final state by a plane wave, the cross section may be expressed as [4]

$$\frac{d\sigma}{d\Omega}=\pi\alpha\frac{p_+(E_++1)}{k}\left\{|\kappa|\left[g^2(q)+\left(\frac{p_+}{E_++1}\right)^2 f^2(q)\right]-2\kappa\frac{p_+}{E_++1}\frac{\cos\theta(k-p_+\cos\theta)}{q}g(q)f(q)\right\}. \quad (10)$$

The momentum transfer q is given in terms of the minimum value [Eq. (6)] and the emission angle θ of the positron relative to the direction of the incoming photon as

$$q^2=q_{\min}^2+2p_+k(1-\cos\theta). \quad (11)$$

$d\Omega=\sin\theta d\theta d\phi$ refers to the emission of the positron. The quantity κ relates to the total angular momentum quantum number j of the populated bound state as $\kappa=\mp(j+\frac{1}{2})$, where the upper sign applies for states where the orbital angular momentum quantum number l of the large component is equal to $j-\frac{1}{2}$ while the lower applies for $l=j+\frac{1}{2}$. The quantities $g(q)$ and $f(q)$ are given in terms of the radial part of the large and small components, $g(r)$ and $f(r)$, of the bound-state spinor,

$$\psi_b(\mathbf{r})=\begin{pmatrix} g_\kappa(r)\Omega_{jlm}(\mathbf{r}/r)\\ if_\kappa(r)\Omega_{j\bar{l}m}(\mathbf{r}/r)\end{pmatrix}, \quad (12)$$

as

$$g(q)=(2/\pi)^{1/2}\int_0^\infty dr\, r^2 g(r) j_l(qr),$$
$$f(q)=(2/\pi)^{1/2}\int_0^\infty dr\, r^2 f(r) j_{\bar{l}}(qr), \quad (13)$$

where j_l denotes a spherical Bessel function of order l and $\bar{l}\equiv l\pm1=j\pm\frac{1}{2}$ (again, the upper and lower signs correspond to upper and lower signs in the relation $l=j\mp\frac{1}{2}$). In Eq. (12) the Ω's are the usual spin-angular bispinors; see, e.g., Refs. [10], [11], or [12].

For the ground state of a hydrogenlike system of atomic number Z, the momentum waves assume the form [11]

$$g(q)=N\frac{1}{q}\frac{\Gamma(s+1)}{(1+q_Z^2)^{(s+1)/2}}\sin[(s+1)\delta],$$
$$f(q)=N\sqrt{\frac{1-s}{1+s}}\frac{1}{q} \quad (14)$$
$$\times\left[\frac{\Gamma(s+1)\cos[(s+1)\delta]}{(1+q_Z^2)^{(s+1)/2}}-\frac{\Gamma(s)\sin(s\delta)}{q_Z(1+q_Z^2)^{s/2}}\right],$$

with $q_Z\equiv q/\alpha Z$, $\delta\equiv\arctan(q_Z)$, $s\equiv\sqrt{1-(\alpha Z)^2}$, and N defined as

$$N=2^{s+1/2}\left(\frac{1+s}{\alpha Z\pi\Gamma(2s+1)}\right)^{1/2}. \quad (15)$$

In the limit $\alpha Z\ll1$, expressions (14) reduce to

$$g(q)=N_0\frac{2}{q}\left(\frac{\alpha Z}{q}\right)^3,$$
$$f(q)=-N_0\left(\frac{\alpha Z}{q}\right)^3, \quad (16)$$

where

$$N_0^2=\frac{8}{\alpha Z\pi}. \quad (17)$$

Integration of Eq. (10) over angles then yields the result

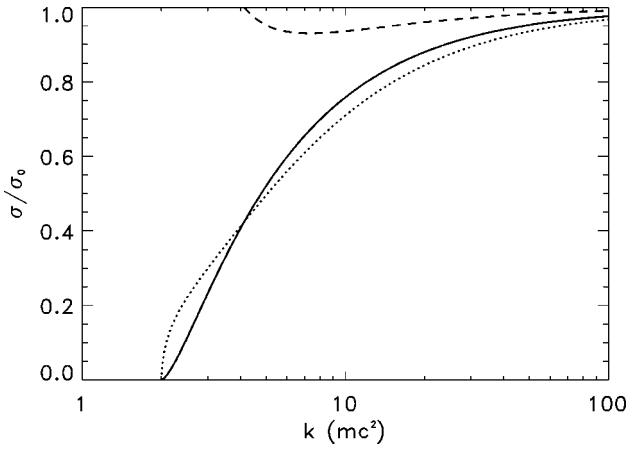

FIG. 1. Cross section for bound-free pair production as a function of the photon energy. The photon is incident on a bare nucleus, and the electron is produced in the ground state of the resulting hydrogenlike atom. The solid curve shows the Sauter expression [Eq. (20)], while the dotted line shows the plane-wave result [Eq. (18)]. Both predictions are divided by the asymptotic cross section σ_0 of Eq. (19). The dashed curve displays the ratio of the plane-wave result to the Sauter result.

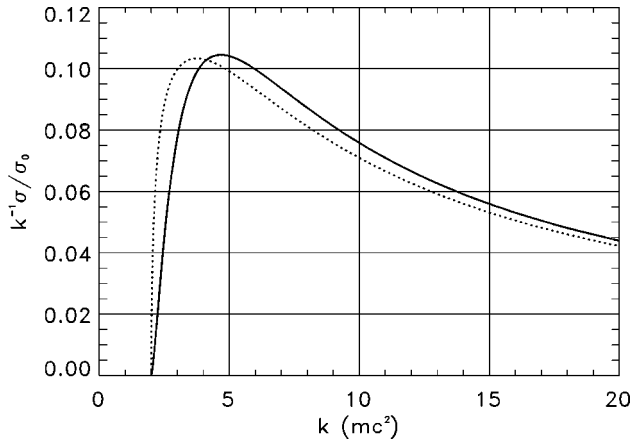

FIG. 2. Cross section for bound-free pair production as a function of the photon energy. As in Fig. 1, the electron is produced in the ground state. The solid curve shows the Sauter expression [Eq. (20)], while the dotted line shows the plane-wave result [Eq. (18)]. Cross sections are shown in units of $4\pi\alpha(\alpha Z)^5\lambda\!\!\!^{-2}_C$.

$$\sigma=\sigma_0\frac{p_+}{k^3}\left(E_+^2-\frac{E_+}{3}+\frac{4}{3}\right). \tag{18}$$

The quantity

$$\sigma_0=\frac{4\pi\alpha(\alpha Z)^5}{k}\lambda\!\!\!^{-2}_C \tag{19}$$

represents the high-energy limit of the cross section, and contains the entire Z dependence at all energies.

Formulas for the photoeffect may be transcribed into formulas for bound-free pair production—and vice versa—by simple substitutions. These involve replacement in matrix elements of the final-state electron momentum and energy by the negative of those of the positron. In addition it should be remembered that the bound-electron state appears as the initial state in the photoeffect but as the final state in the pair creation process. Transcription of Sauter's result for the photoeffect gives a cross section for pair creation, with the electron produced directly in the $1s$ state, of [13]

$$\sigma=\sigma_0\frac{p_+^3}{k^4}\left(-\frac{4}{3}+\frac{E_+(E_++2)}{E_+-1}\times\left[1-\frac{1}{2E_+p_+}\ln\frac{E_++p_+}{E_+-p_+}\right]\right). \tag{20}$$

In the extreme high-energy limit, expression (20) also reduces to σ_0, and again there is no dependence on Z other than that contained in σ_0.

Figures 1 and 2 show a comparison of the plane-wave result [Eq. (18)] and the transcribed Sauter formula [Eq. (20)]. Figure 1 displays the two predictions for the cross section, both divided by the high-energy result σ_0 [Eq. (19)], as well as their ratio. At high energies both predictions approach the asymptotic formula, that is, they decrease roughly as $1/k$. Beyond twice the threshold energy, they differ by less than 10% from each other. Differences are mainly confined to the first two units above threshold. Figure 2 shows the predictions for the cross section directly without dividing out the asymptotic energy dependence. The cross section displays a peak at relatively low energy, and differences are mainly confined to the region near and below this maximum. In this narrow region, on the other hand, the ratio between the two predictions may become quite large.

Besides the fact that Sauter's formula actually is applicable only for the very lightest targets (cf. Ref. [10]), the relatively large differences encountered near and below the production maximum for the Coulomb case are of no major concern in relation to the production of pairs of heavy leptons: For heavy leptons finite nuclear size gives a strong suppression exactly in the region, where major differences are encountered for the Coulomb potential between the plane-wave approach and Sauter's approach, which includes lowest-order corrections to the bound wave. As an example, for production of a μ pair on a uranium nucleus with the negatively charged lepton bound in the ground state, the maximum cross section as computed in the plane-wave approach appears at an energy of 7.8. This is much higher than the positions of the plane-wave maximum for the Coulomb case and the Sauter maximum, which appear at 3.8 and 4.7; cf. Fig. 2. The plane-wave approximation is expected to be sufficiently accurate, and no expansion of the wave function for the positively charged lepton is presumably needed, when we have moderate variations of the potential over the Compton wavelength of the particle in question (that is, when the Coulomb divergence is avoided). For μ and τ production, corrections due to nonperturbative as well as Sauter-type effects are much smaller than those due to finite nuclear size.

B. Photoelectric effect

Transcription of the cross section for bound-free pair creation obtained above [Eq. (18)] to the case of the photoeffect gives

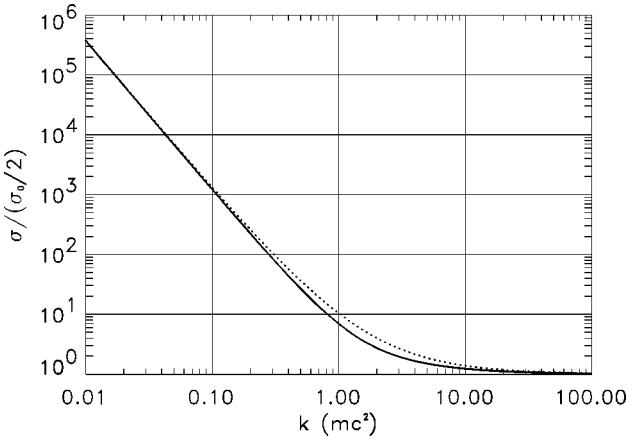

FIG. 3. Cross section for the photoeffect for a hydrogenlike system in the ground state as a function of the photon energy. The solid curve shows the Sauter expression [Eq. (22)] while the dotted line shows the plane-wave result [Eq. (21)]. Both predictions are divided by the asymptotic cross section $\sigma_0/2$, where σ_0 is defined by Eq. (19).

$$\sigma = \frac{\sigma_0}{2}\frac{p}{k^3}\left(E^2 + \frac{E}{3} + \frac{4}{3}\right), \tag{21}$$

where E denotes the total relativistic energy and p the momentum of the electron in the final state; also see Ref. [14]. The factor of $\frac{1}{2}$ in front is due to the fact that only a single electron occupies the K shell when we consider a hydrogenlike system. The factor did not appear in the case of bound-free pair creation since, there, we allow production of a bound electron in any of the two $1s$ states. Sauter's result, on the other hand, reads

$$\sigma = \frac{\sigma_0}{2}\frac{p^3}{k^4}\left(\frac{4}{3} + \frac{E(E-2)}{E+1}\left[1 - \frac{1}{2Ep}\ln\frac{E+p}{E-p}\right]\right). \tag{22}$$

At high energies, both expressions (21) and (22) approach $\sigma_0/2$; that is, the same high-energy limit's obtained as in the case of pair creation (except for the factor of 1/2).

Figure 3 shows a comparison of the plane-wave result [Eq. (21)] and Sauter's expression [Eq. (22)] over a wide range of photon energies. Remarkably, the two results approach each other at both ends of the energy scale. In particular, in the limit of small energies they both approach the standard nonperturbative result pertaining to nonrelativistic energies; see, e.g., Heitler [7] for an explicit expression. At intermediate energies, the plane-wave result is higher than the Sauter cross section. This is spelled out in Fig. 4, which displays the ratio between the two. Differences are moderate, attaining a maximum of slightly above 1.5 at a photon energy slightly above mc^2.

While differences between the total cross sections are moderate, the differences between the differential cross sections obtained with the plane-wave approach and by Sauter are substantial at high energies. For a photon moving along the z axis and linearly polarized in the direction of the x axis,

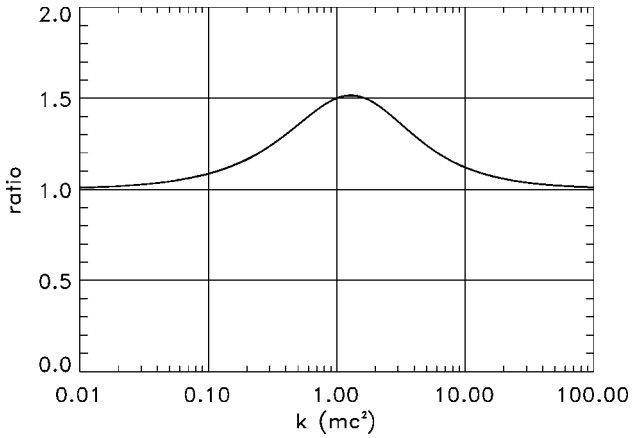

FIG. 4. Ratio of the plane-wave result [Eq. (21)] and the Sauter expression [Eq. (22)] for the K-shell photoeffect as a function of the photon energy.

the result for the emission of an electron with polar and azimuthal angles θ and ϕ, as obtained in the plane-wave description, reads

$$\frac{d\sigma}{d\Omega} = \frac{\sigma_0}{2\pi}\frac{p(E+1)}{k^3E^4}\left[\frac{\sin^2\theta\cos^2\phi}{(1-\beta\cos\theta)^4} + \frac{E(E-1)}{4(E+1)}\frac{1}{(1-\beta\cos\theta)^3}\right], \tag{23}$$

where $\beta = p/E$ is the speed of the ejected electron; also see Ref. [14]. On the other hand, Sauter's result reads [9,15]

$$\frac{d\sigma}{d\Omega} = \frac{\sigma_0}{2\pi}\frac{p^3}{k^4E^4}\left[\frac{\sin^2\theta\cos^2\phi}{(1-\beta\cos\theta)^4} - \frac{E(E-1)}{2}\frac{\sin^2\theta\cos^2\phi}{(1-\beta\cos\theta)^3} + \frac{E(E-1)^2}{4}\frac{\sin^2\theta}{(1-\beta\cos\theta)^3}\right]. \tag{24}$$

In the nonrelativistic region, both cross sections are dominated by the first term in square brackets, and in the limit of small photon energies formulas (23) and (24) produce identical results. At high energies, the last term, which permits emission in directions perpendicular to the photon polarization, dominates in both cases. Upon integration over angles this term alone yields the high-energy limit $\sigma_0/2$, while the other terms give contributions which depend on the photon energy as $1/k^2$, that is, the contribution to the total cross section of the first terms relative to that of the last term decreases as $1/k$. We note, furthermore, that the characteristic angle of emission at high energies is $1/k$. Otherwise the distributions are quite different here: while the plane-wave result [Eq. (23)] produces a maximum for forward emission at high energies, Sauter's cross section [Eq. (24)] vanishes for $\theta = 0$ at all energies. As a result the Sauter distribution [Eq. (24)] is broader than the plane-wave result [Eq. (23)]. According to Eq. (24) one-fourth of the emission appears for angles smaller than $1/k$ at high energies, while three-fourths of the total cross section pertain to emission angles larger than $1/k$. For the plane-wave result [Eq. (23)] the result is the

exact opposite. In the high-energy limit the two expressions (23) and (24) cross over at $\theta = 1/k$.

Although the differences between the differential cross sections are substantial at high energies, as explained above, they are actually not of concern for the investigation of the impact-parameter dependence of the process. The reason for this is simply that, when squeezing down the packet to have a spatial resolution on the scale of the Compton wavelength, an angular divergence of the packet in excess of $1/k$ is implied. Hence the differences discussed above are completely smeared out. In addition to this we may add that exact calculations of the photoeffect for high energies again yield a nonzero cross section for forward emission. The relative magnitude of the cross section for $\theta = 0$ increases with the atomic number Z, such as to produce a maximum in the limit where also Z is high.

To sum up Sec. III, we have seen that while the plane-wave approach is not perfect, it is certainly sufficient for analyzing the spatial resolution of high-energy photoprocesses.

IV. WAVE-PACKET ANALYSIS OF THE PHOTOEFFECT

A. Theoretical model

To prepare for a direct computation of the impact-parameter dependence of the photoeffect, consider an initial quantum state composed of a one-photon wave packet and an electron bound in the ground state of hydrogen-like system:

$$|\text{initial}\rangle = \frac{1}{(2\pi)^{3/2}} \sum_{i=1}^{2} \int d^3k\, g_i(\mathbf{k}) |\mathbf{k}i, 1s\rangle. \tag{25}$$

Here i indicates the direction of photon polarization, and the amplitudes g_i are normalized as

$$\sum_{i=1}^{2} \int d^3k |g_i(\mathbf{k})|^2 = 1. \tag{26}$$

The factor of $(2\pi)^{-3/2}$ is due to a plane-wave representation of the form $\exp(i\mathbf{k}\cdot\mathbf{r})$ where $\mathbf{k}$ denotes the photon momentum; see, e.g., Ref. [16]. The final state consists, in principle, of a superposition of states with any number of photons. However, as we shall restrict our treatment to a perturbation calculation of lowest order, the final state encountered after photoejection of the electron contains no photons. Hence we write

$$|\text{final}\rangle = |0, \psi_e\rangle, \tag{27}$$

where the electron state assumes the form

$$\psi_e = \sum c_n \psi_n + \sum_{m_s=-1/2}^{+1/2} \frac{1}{(2\pi)^{3/2}} \int d^3p\, c_{\mathbf{p}m_s} \psi_{\mathbf{p}m_s}, \tag{28}$$

the first sum being over bound states. We shall approximate the unbound electron waves by simple plane-wave spinors

$$\psi_{\mathbf{p}m_s} = \sqrt{\frac{E+1}{2E}} \begin{pmatrix} \chi_{m_s} \\ \dfrac{\boldsymbol{\sigma}\cdot\mathbf{p}}{E+1} \chi_{m_s} \end{pmatrix} e^{i\mathbf{p}\cdot\mathbf{r}}, \tag{29}$$

the corresponding density in momentum space of expansion (28) being $|c_{\mathbf{p}m_s}|^2$. In Eq. (29), $\boldsymbol{\sigma} = (\sigma_x, \sigma_y, \sigma_z)$ is the Pauli spin matrix, and χ_{m_s} denotes a Pauli spinor,

$$\chi_{1/2} = \begin{pmatrix} 1 \\ 0 \end{pmatrix}, \quad \chi_{-1/2} = \begin{pmatrix} 0 \\ 1 \end{pmatrix}. \tag{30}$$

Although the states of Eqs. (29) and (30) in general are not eigenstates of the spin-projection operator, we shall term them ''spin-up'' and ''spin-down.'' As an alternative we could have chosen a basis consisting of the two helicity eigenstates, but there is no particular reason in relation to the present investigation to make this choice.

With the states of Eqs. (25) and (27)–(29) we perform a first-order perturbation calculation for the transition of the electron from the ground state of energy $E_{1s} = \sqrt{1-(\alpha Z)^2}$ to a final unbound state of momentum $\mathbf{p}$, spin projection m_s, and energy $E = \sqrt{p^2+1}$ under the absorption of a photon. This gives

$$i(2\pi)^{3/2} \frac{d}{dt} c_{\mathbf{p}m_s} = \frac{1}{(2\pi)^{3/2}} \sum_{i=1}^{2} \int d^3k\, g_i(\mathbf{k}) \times M_{\mathbf{p}m_s, \mathbf{k}i} e^{i(E-E_{1s}-k)t}, \tag{31}$$

where the matrix element is given by the standard expression [7]

$$M_{\mathbf{p}m_s, \mathbf{k}i} = e \sqrt{\frac{2\pi}{k}} \int d^3r\, \psi^{\dagger}_{\mathbf{p}m_s} \alpha_i e^{i\mathbf{k}\cdot\mathbf{r}} \psi_{1s}, \tag{32}$$

α_i being the projection of the Dirac $\boldsymbol{\alpha}$ matrix in the polarization direction i. The photon wave packet is in closest proximity of the center of the atom at $t = 0$. Hence, when integrating Eq. (31) over time, we extend the interval of integration from $t \to -\infty$ to $t \to +\infty$. A δ function with argument $E - E_{1s} - k$ then results, and the coefficient $c_{\mathbf{p}m_s}$ assumes, after the passage of the packet, the value

$$c_{\mathbf{p}m_s}(t \to \infty) = \frac{8\pi^2 (E-E_{1s})^2}{(2\pi)^3 i} M_0, \tag{33}$$

where we have introduced the quantity

$$M_0 = \frac{1}{4\pi} \int_{4\pi} d\Omega_{\mathbf{k}} \sum_{i=1}^{2} g_i(\mathbf{k}) M_{\mathbf{p}m_s, \mathbf{k}i} \Big|_{k=E-E_{1s}}. \tag{34}$$

With a momentum-space density of $|c_{\mathbf{p}m_s}|^2$, the differential probability for the photoconversion to happen and produce an outgoing electron of momentum $\mathbf{p}$ and spin projection m_s is simply $|c_{\mathbf{p}m_s}(t \to \infty)|^2$, that is,

$$\frac{dP}{d^3p}=\pi^{-2}(E-E_{1s})^4|M_0(k=E-E_{1s})|^2. \tag{35}$$

Note that the photon distribution (g) entering M_0 need not be centered at the energy $k=E-E_{1s}$ (or vice versa).

To proceed to the actual calculations, we shall now make a specific choice for the photon amplitudes g_i. We choose

$$g_i(\mathbf{k})=c_i\left(\frac{2\Delta}{\pi}\right)^{3/4}e^{-i\mathbf{k}\cdot\mathbf{b}}e^{-\Delta(\mathbf{k}-\mathbf{k}_0)^2}, \tag{36}$$

where $\Delta>0$, and

$$|c_1|^2+|c_2|^2=1, \quad \mathbf{k}_0\cdot\mathbf{b}=0; \tag{37}$$

that is, we consider a packet which moves on average with momentum $\mathbf{k}_0$ and which approaches the atom at an impact parameter of b. We further choose

$$\mathbf{e}_z=\mathbf{k}_0/k_0, \quad \mathbf{e}_x=\mathbf{b}/b, \quad \mathbf{e}_y=\mathbf{e}_z\times\mathbf{e}_x \tag{38}$$

as the basis for our coordinate system. For the polarization directions i of the individual photons we choose $\mathbf{e}_1$ to be in the plane spanned by $\mathbf{b}$ and $\mathbf{k}$, while $\mathbf{e}_2=\mathbf{k}\times\mathbf{e}_1/k$. With this choice, the projections of the Dirac matrices appearing in Eq. (32) assume the form

$$\alpha_1=\frac{k_{yz}}{k}\alpha_x-\frac{k_xk_y}{k_{yz}k}\alpha_y-\frac{k_xk_z}{k_{yz}k}\alpha_z, \tag{39}$$

$$\alpha_2=\frac{k_z}{k_{yz}}\alpha_y-\frac{k_y}{k_{yz}}\alpha_z, \tag{40}$$

where, for short, we have introduced the notation $k_{yz}=(k_y^2+k_z^2)^{1/2}$. For small transverse momentum spreads the two projections are close to α_x and α_y.

Upon insertion of a plane wave [Eq. (29)] for the final electron state, the matrix element [Eq. (32)] reduces essentially to the Fourier transform of the initial bound-state wave function. With the definition

$$\psi(\mathbf{q}')=\frac{1}{(2\pi)^{3/2}}\int d^3r\,\psi(\mathbf{r})e^{-i\mathbf{q}'\cdot\mathbf{r}}, \tag{41}$$

the Fourier transform of ψ_b of Eq. (12) assumes the form

$$\psi_b(\mathbf{q}')=i^{-l}\begin{pmatrix} g(q')\Omega_{jlm}(\mathbf{q}'/q') \\ -S_\kappa f(q')\Omega_{j\bar{l}m}(\mathbf{q}'/q')\end{pmatrix}, \tag{42}$$

where $S_\kappa\equiv\kappa/|\kappa|$, and $g(q')$ and $f(q')$ are defined in Eq. (13); cf. Ref. [11]. Hence, by insertion of expressions (12) and (29), the matrix element [Eq. (32)] may be recast in the form

$$M_{\mathbf{p}m_s,\mathbf{k}i}=C\begin{pmatrix}\chi_{m_s}\\ \dfrac{\boldsymbol{\sigma}\cdot\mathbf{p}}{E+1}\chi_{m_s}\end{pmatrix}^\dagger\alpha_i\begin{pmatrix} g(q)\Omega_{jlm}(-\mathbf{q}/q)\\ -S_\kappa f(q)\Omega_{j\bar{l}m}(-\mathbf{q}/q)\end{pmatrix}, \tag{43}$$

where $\mathbf{q}\ (=-\mathbf{q}')$ is the recoil momentum [Eq. (4)], and

$$C=(2\pi)^{3/2}i^{-l}e\sqrt{\frac{2\pi}{k}}\sqrt{\frac{E+1}{2E}}. \tag{44}$$

In the further computation, let us assume the electron originally to be in the $1s$ spin-up state, whereby

$$\Omega_{jlm}(-\mathbf{q}/q)=\frac{1}{\sqrt{4\pi}}\begin{pmatrix}1\\0\end{pmatrix}, \tag{45}$$

$$\Omega_{j\bar{l}m}(-\mathbf{q}/q)=\frac{1}{\sqrt{4\pi}}\begin{pmatrix}q_z/q\\(q_x+iq_y)/q\end{pmatrix}, \tag{46}$$

and $\kappa=-1$. Since α_i appearing in the matrix element [Eq. (43)] is a linear combination of α_x, α_y, and α_z, let us list the explicit results for Eq. (43) when either of these components is substituted for α_i. Not including the factor $C/\sqrt{4\pi}$, the results are

$$g(q)\frac{p_x-ip_y}{E+1}+f(q)\frac{q_x+iq_y}{q}, \quad \alpha_x\uparrow \tag{47}$$

$$-g(q)\frac{p_z}{E+1}+f(q)\frac{q_z}{q}, \quad \alpha_x\downarrow \tag{48}$$

$$g(q)\frac{ip_x+p_y}{E+1}-f(q)\frac{iq_x-q_y}{q}, \quad \alpha_y\uparrow \tag{49}$$

$$-g(q)\frac{ip_z}{E+1}+f(q)\frac{iq_z}{q}, \quad \alpha_y\downarrow \tag{50}$$

$$g(q)\frac{p_z}{E+1}+f(q)\frac{q_z}{q}, \quad \alpha_z\uparrow \tag{51}$$

$$g(q)\frac{p_x+ip_y}{E+1}-f(q)\frac{q_x+iq_y}{q}, \quad \alpha_z\downarrow. \tag{52}$$

Here $\uparrow$ indicates spin-up in the final electron state, while $\downarrow$ indicates spin-down. The functions $g(q)$ and $f(q)$ are given in Eq. (14).

B. Results

We now have all the ingredients to compute the differential probability for photoconversion. We apply Eq. (35) and use expressions (34), (36), (43)–(44), (39)–(40), and (47)–(52), the latter with Eqs. (14) and (15). All calculations are done for linearly polarized photons, that is, we make the choices $c_1=1$ and $c_2=0$ in Eq. (36). Except for a single case we choose to work with low Z. This in essence has two reasons. First, by application of the plane-wave approach we are doing a perturbation calculation. This demands low Z. From Ref. [10] we actually know that the perturbative cross section is already off relative to the exact value by something like 20% in the high-energy limit for $Z=8$. Second, if the length scale is the Compton wavelength rather than the radius of the atomic $1s$ state, then this should appear most

clearly for low atomic numbers, where the difference between the two is up to two orders of magnitude.

Before exploring the impact-parameter dependence, let us demonstrate how our wave-packet calculation conforms to the differential cross sections discussed in Sec. III, Eqs. (23) and (24). For this we will need a procedure for converting our results to differential cross sections. For the moment, assume that the packet [Eq. (36)] has different widths along and transverse to the direction of $\mathbf{k}_0$ corresponding to two different values of the quantity Δ; we shall call these Δ_z and $\Delta_\perp$. Let us assume the packet to be very wide, so that it is essentially uniform over the struck atom; that is, we assume $\Delta \gg 1$. For a photon described by such a packet, the probability for photoelectron emission in a given direction may be expressed in two equivalent ways,

$$\frac{d\sigma}{d\Omega}\frac{1}{2\pi\Delta_\perp} = \int dp\, p^2 \frac{dP}{d^3p}, \tag{53}$$

the factor on the cross section being the photon density integrated along the direction of $\mathbf{k}_0$. On the right-hand side, $E\,dE = E\,dk$ may be substituted for pdp, and, for the packet, which is exceedingly narrow in momentum space, the factor pE may be taken outside the integral with a value equal to the product of $E = k_0 + E_{1s}$ and $p = (E^2-1)^{1/2}$. The remaining integral assumes, for the packet that is narrow in momentum, the value of the differential probability at the center of the distribution, again corresponding to $E = k_0 + E_{1s}$ times $(\pi/2\Delta_z)^{1/2}$. With Eq. (35) our result for the differential cross section then reads

$$\frac{d\sigma}{d\Omega} = pEk_0^4\Delta_\perp \sqrt{\frac{2}{\pi\Delta_z}}|M_0|^2, \quad k = k_0 = E - E_{1s}. \tag{54}$$

In applications of Eq. (54) it is understood that M_0 must be computed for a packet which is wide in direct space (narrow in momentum), $\Delta \gg 1$.

Figure 5 displays our result [Eq. (54)] for the differential cross section for a very broad photon packet, $\Delta = 1\times10^9$, incident at low energy, $0.01mc^2$, on a hydrogen atom. The variation of the cross section with polar emission angle θ is shown for a vanishing azimuthal angle ϕ (as measured relative to the direction of photon polarization) and, of course, a vanishing impact parameter. The full-drawn curve is the sum over spin projections for the emitted electron. However, this sum is practically identical to the result for the spin-up direction while the spin-flip contribution essentially vanishes. The latter is indicated as a dotted line which runs along the horizontal axis of the plot. In the figure we also plot the Sauter distribution [Eq. (24)]. Clearly the two are very close as expected at this low energy. We have not attempted to display the plane-wave result [Eq. (23)], as this is indistinguishable from our numerical result in the considered case.

Figure 6 similarly displays our result [Eq. (54)] for the differential cross section for a very broad photon packet, $\Delta = 1\times10^6$, now incident at high energy, $100mc^2$, on a hydrogen atom. The cross section, multiplied by sin θ, is shown as a function of the polar emission angle θ for $\phi = 0$ and a vanishing impact parameter. The cross section summed over

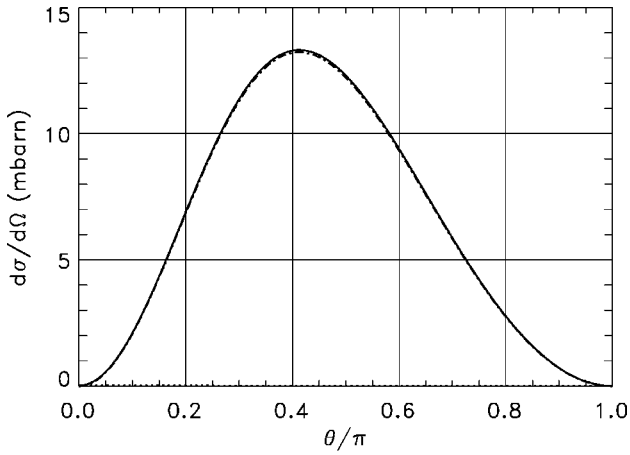

FIG. 5. Differential cross section for the photoeffect at low energy, $k_0 = 0.01$. The cross section is shown as a function of the polar emission angle θ for impact of a linearly polarized photon on a hydrogen atom, which is in the ground state. The full-drawn curve is our numerical result, summed over final spin directions, for a wide packet $\Delta = 1\times10^9$ at a vanishing impact parameter $b = 0$, while the chained curve displays the Sauter distribution [Eq. (24)]. The azimuthal emission angle is set to zero, $\phi = 0$.

spin projections (full-drawn curve) is now dominated by the spin-flip contribution (dotted curve) except at large angles, where the cross section becomes small. The Sauter result (chained curve) is now quite different from our result, as expected, but integrated values are close. Note that our cross section is finite at $\theta = 0$ due to the spin-flip contribution, while Sauter's result as well as our spin-up contribution vanish here. We do not show the analytical plane-wave result [Eq. (23)] in the figure. Due to the finite value of Z it is slightly different from our numerical result; differences

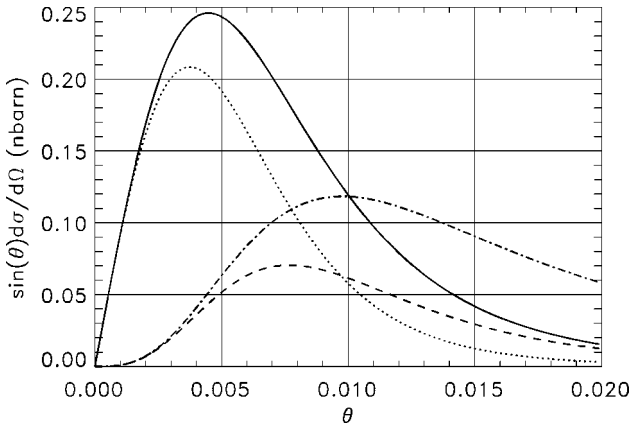

FIG. 6. Differential cross section for the photoeffect at high energy, $k_0 = 100$. The cross section, times sin θ, is shown as a function of the polar emission angle θ for impact of a linearly polarized photon on a hydrogen atom, which is in the ground state. The full-drawn curve is our numerical result, summed over final spin directions, for a wide packet $\Delta = 1\times10^6$ incident at a vanishing impact parameter $b = 0$, while the dashed and dotted curves break the total up into spin-up and spin-flip contributions. The chained curve displays the Sauter distribution [Eq. (24)]. The azimuthal emission angle is set to zero, $\phi = 0$.

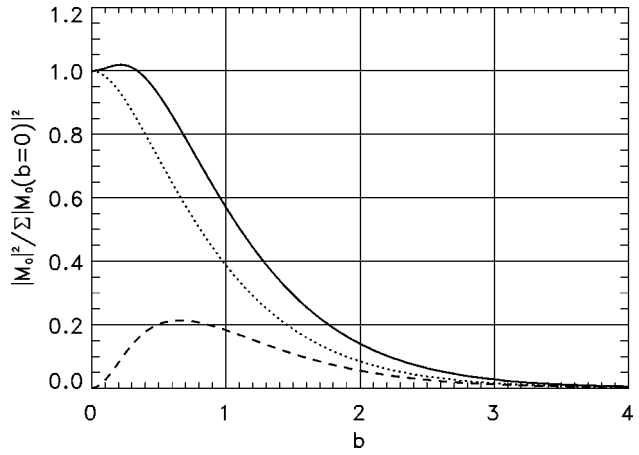

FIG. 7. Impact-parameter dependence of the photoelectric effect at high energy, $k_0=1000$. The figure shows the probability of emitting an electron at a polar angle $\theta=0.001$ and an azimuthal angle $\phi=0$ as a function of b for a narrow packet $\Delta=0.01$, incident on a hydrogen atom $Z=1$ in the ground state. The full-drawn curve shows the probability summed over spin directions of the outgoing electron, while the dotted and dashed curves display the spin-flip and spin-up contributions. All curves are normalized to the value of the sum at $b=0$, and the impact parameter is given in units of $\lambda\!\!\!^{-}_C$, the Compton wavelength of the electron.

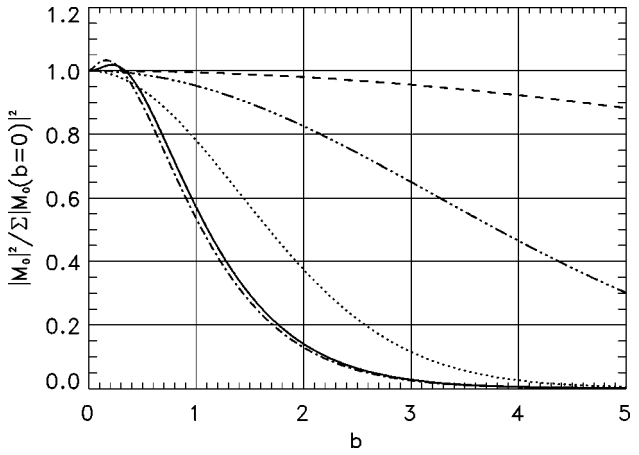

FIG. 8. Influence of the width of the wave packet on distribution over the impact parameter. The figure shows the total probability for emitting an electron at a polar angle $\theta=0.001$ and an azimuthal angle $\phi=0$ as a function of b for packets of varying widths centered at $k_0=1000$ incident on a hydrogen atom. The atom is initially in the ground state. The values of Δ are 0.0001 (chained curve), 0.01 (full-drawn curve), 1 (dotted), 10 (triple-dot-dashed), and 100 (dashed). All curves are normalized to their respective values at $b=0$, and the impact parameter is given in units of $\lambda\!\!\!^{-}_C$.

amount to 1% near the maximum in the figure, and decrease with increasing angle. The differences between the two approaches may be removed by setting Z artificially low.

Having successfully tested our wave-packet approach against the analytical results Eqs. (23) and (24), let us now turn to an investigation of the impact-parameter dependence. Figure 7 shows the production probability [Eq. (35)] for photoelectrons as a function of b for a high-energy photon incident on a hydrogen atom. The photon energy is centered at $k_0=1000(mc^2)$, the electron energy is chosen as $E=k_0+E_{1s}$, and the emission angle is chosen as $1/k_0$, which is characteristic of the emission at high energy. The incident wave packet is narrow in direct space, $\Delta=0.01$. The figure shows the production probability summed over spin directions of the outgoing electron as well as the individual spin-up ($m_s=\frac{1}{2}$) and spin-flip ($m_s=-\frac{1}{2}$) contributions, all normalized to the total probability at head-on impact, $b=0$. Production with spin-flip dominates in the region where production is high. As is immediately apparent from the figure, the photoelectron production varies on the scale of the Compton wavelength. There is absolutely no trace of the extent of the atom, which is measured by the Bohr radius a_0, totaling $\alpha^{-1}\lambda\!\!\!^{-}_C\simeq 137\lambda\!\!\!^{-}_C$.

The influence of the width of the wave packet on the distribution of production probability over impact parameter is shown in Fig. 8. The figure displays the production probability summed over spin directions of the outgoing electron for widths Δ ranging from 0.0001 to 100. As in Fig. 7, a hydrogen atom is struck, the photon energy is centered at $k_0=1000\,(mc^2)$, the electron energy is chosen as $E=k_0+E_{1s}$, and the emission angle is chosen as $1/k_0$. As expected, the width of the distribution in impact parameter broadens when Δ increases, since this implies a narrowing in momentum space and thereby a broadening in direct space. One implication of this smearing is that the spin-up contribution does not vanish near $b=0$ for wide packets, as is the case for narrow packets (cf. Fig. 7). It is obvious that the full-drawn curve, which is repeated from Fig. 7 and computed for $\Delta=0.01$, essentially represents the ultimate resolution in impact parameter.

Decreasing the wave-packet width in direct space (that is, decreasing the value of Δ) inevitably implies a broadening in momentum space. Hence the high resolution in the impact parameter, found in Fig. 8 for small values of Δ, is obtained at the expense of a widening in the distribution over angles for the emitted electron. This is displayed in Fig. 9, which shows the angular distributions recorded at $b=1$ for a broad range of wave-packet widths for the same settings as in Fig. 8. For the widest packet, $\Delta=100$, the distribution is very close to the result (23), which is shown by the thin solid line (narrow distribution). A comparison of Figs. 8 and 9 reveals that the choice $\Delta=1$ allows for reasonable resolution in both impact parameter and angle, that is, resolution on the scales of $\lambda\!\!\!^{-}_C$ and $1/k_0$.

Figure 7 showed no indication that the spatial distribution of the initial electron wave function (in the considered case the rather wide $1s$ hydrogen state) plays any role in the spatial distribution of the photoelectric effect. Hence we expect the distribution of the latter to be essentially Z independent. This is revealed by Fig. 10, which shows total production probabilities for a high-energy photon incident on hydrogenlike $1s$ systems with Z values of 1, 10, and 92. Except for the value of Z, the settings are as in Fig. 7. The variation of the distribution over impact parameter with Z is modest, within a factor of roughly 2, over the entire range of atomic numbers, with the highest Z value displaying the narrowest distribution. At this point it should of course be kept in mind that the

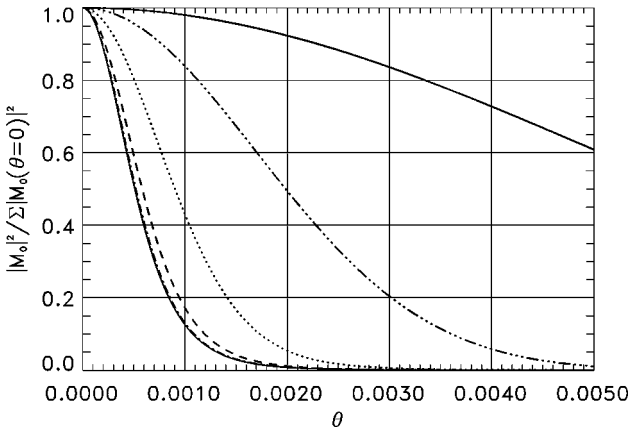

FIG. 9. Influence of the width of the wave packet on distribution over the emission angle. The figure shows the total probability for packets of varying widths centered at $k_0=1000$ incident on a hydrogen atom as a function of the polar emission angle θ of the photoelectron for an azimuthal emission angle of $\phi=0$ and an impact parameter of $b=1$. The atom is initially in the ground state. The values of Δ are 0.01 (full-drawn curve), 0.1 (triple-dot-dashed curve), 1 (dotted curve), 10 (dashed curve), and 100 (chained curve). The thin full-drawn line displaying the the narrowest distribution is the plane-wave result [Eq. (23)]. All curves are normalized to their respective values at $\theta=0$, and the impact parameter is given in units of $\lambda\!\!\!^{-}_C$.

plane-wave calculation of the total cross section is off by a factor of, roughly, 5 at the considered energy for the highest Z value displayed (cf. Ref. [10]), so that, although there is no particular reason to believe this influences the distribution over impact parameter in any major way, details should of course be interpreted with care.

In our last figure, Fig. 11, we demonstrate that the dominance of distances of the order of the Compton wavelength in the photoeffect also holds at moderate energies. In other words, the Compton scale does not only appear at excessively high energies. As in Fig. 7 a photon is incident on a hydrogen atom, but the energy is now centered at $k_0=1\,(mc^2)$, the polar emission angle is $\theta=1$, and the width of the packet is chosen as $\Delta=5$; other settings are unchanged. The figure shows the very clear dominance of the Compton scale. Again, there is absolutely no trace of the extent of the atom. It may be noted that the variation of the total production probability for given width, e.g., $\Delta=10$, turns out to be roughly the same at $k_0=1$ and 1000, except that the roles of the spin-up and spin-flip contributions are inverted; the former dominates at lower energy, while the latter dominates at higher energy.

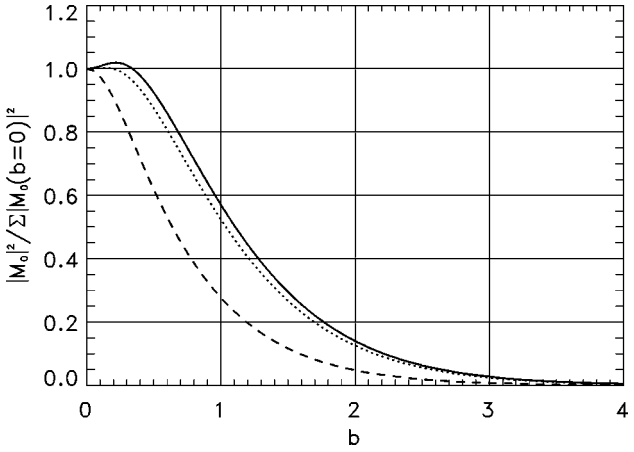

FIG. 10. Influence of the atomic number on distribution of the photoeffect over impact parameter. The figure shows the total probability as a function of the impact parameter for photons incident on hydrogenlike systems of different atomic numbers $Z=1$ (full-drawn curve), $Z=10$ (dotted curve), and $Z=92$ (dashed curve). Other settings are as in Fig. 7.

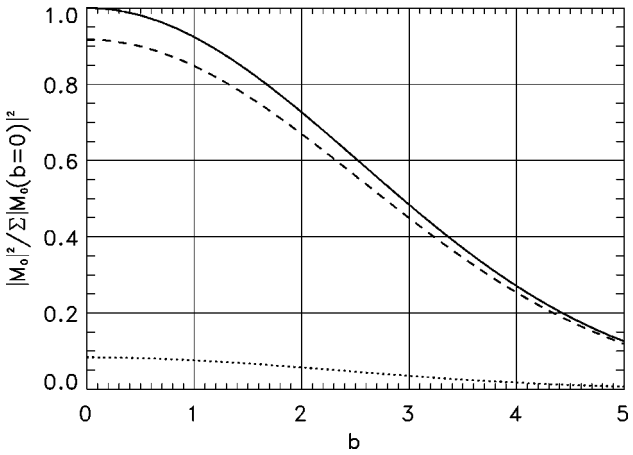

FIG. 11. Impact-parameter dependence of the photoelectric effect at moderate energy, $k_0=1$. The figure shows the probability for emitting an electron at a polar angle $\theta=1$ and an azimuthal angle $\phi=0$ as a function of b for a packet with $\Delta=5$, incident on a hydrogen atom $Z=1$ in the ground state. Curves and normalization are as in Fig. 7.

V. CONCLUSION

The wave-packet approach applied above has demonstrated very clearly, and in a very direct way, that, at relativistic energies, photoelectric conversion takes place only in a narrow region around the Coulomb center. The extent of the initial electron state is immaterial: the scale is the Compton wavelength of the electron. The analysis confirms expectations based on simple arguments on recoil momenta. In addition, it provides a detailed picture of the impact-parameter dependence of the photoelectric effect.

For pair creation the arguments on recoil momenta show that while production with bound electron only involves distances of order $\lambda\!\!\!^{-}_C$ from the nucleus, exactly like the photoeffect, the creation of pairs of free (unbound) particles involves the entire atom in the high-energy limit. (As opposed to the case of bremsstrahlung, this limit is not approached until the primary energy becomes very high—typically beyond 100 MeV). While true, this could seem to be turned upside down, since in pair production with bound electron a specific atomic orbital is involved.

In closing, let us mention that our analysis suggests that nonperturbative corrections will be larger for pair creation with bound electron and the photoeffect, as compared to the

production of free pairs and bremsstrahlung emission by energetic electrons and positrons in atomic fields, due to localization in the region of strongest field. This observation is in agreement with actual findings.

ACKNOWLEDGMENT

This work was supported by the Danish Natural Science Research Council.

[1] J. D. Jackson, *Classical Electrodynamics* (Wiley, New York, 1975).
[2] M. L. Ter-Mikaelian, *High-Energy Electromagnetic Processes in Condensed Media* (Wiley, New York, 1972).
[3] R. H. Pratt, Akiva Ron, and H. K. Tseng, Rev. Mod. Phys. **45**, 273 (1973).
[4] A. Belkacem and A. H. Sørensen, Phys. Rev. A **57**, 3646 (1998).
[5] A. H. Sørensen, Phys. Rev. A **55**, 2896 (1997).
[6] O. Keller, Phys. Rev. A **62**, 022111 (2000). Also see references therein, as well as I. Bialynicki-Birula, Phys. Rev. Lett. **80**, 5247 (1998).
[7] W. Heitler, *The Quantum Theory of Radiation* (Dover, New York, 1984).
[8] V. B. Berestetskii, E. M. Lifshitz, and L. P. Pitaevskii, *Quantum Electrodynamics* (Pergamon Press, New York, 1989).
[9] F. Sauter, Ann. Phys. (Leipzig) **11**, 454 (1931).
[10] C. K. Agger and A. H. Sørensen, Phys. Rev. A **55**, 402 (1997).
[11] A. H. Sørensen and A. Belkacem, Phys. Rev. A **49**, 81 (1994).
[12] W. Greiner, *Relativistic Quantum Mechanics—Wave Equations* (Springer, Berlin, 1990).
[13] By mistake, formula (52) quoted in Ref. [10] is the formula for the photoeffect. To obtain the corresponding result for bound-free pair creation E_+ and p_+ appearing in Eq. (52) in [10] should be replaced by $-E_+$ and $-p_+$.
[14] K. W. McVoy, Phys. Rev. **108**, 365 (1957).
[15] R. H. Pratt, R. D. Levee, R. L. Pexton, and W. Aron, Phys. Rev. **134**, A898 (1964).
[16] C. Cohen-Tannoudji, J. Dupont-Roc, and G. Grynberg, *Atom-Photon Interactions* (Wiley, New York, 1992).